Flame Synthesis of Metal-Catalyzed Single-Wall Carbon Nanotubes

Randall L. Vander Wal*

NCMR c/o NASA-Glenn, M.S. 110-3, 21000 Brookpark Road, Cleveland, Ohio 44135

Thomas M. Ticich and Valerie E. Curtis

Centenary College of Louisiana, Department of Chemistry, 2911 Centenary Boulevard, Shreveport, Louisiana 71134

Received: December 7, 1999; In Final Form: May 1, 2000

In the work presented here, flame conditions are tailored to create a synergy between various metallic additives (cobaltocene, nickelocene, cobalt acetylacetonate, and ferrocene) and the flame environment to synthesize the desirable product of single-wall carbon nanotubes. The flame conditions for synthesis of the nanotubes is explored by using C_2H_2, C_2H_4 and CO in combination with H_2, CH_4 or air along with an inert carrier (He, N_2 or Ar) over a range of concentrations. Possible mechanisms for the encapsulation of the particles within a carbonaceous matrix are considered.

Introduction

Carbon nanotubes are predicted to possess novel mechanical and electrical properties owing to both their regular, periodic structure and quantum size.[1−3] Applications to date have included scanning tunneling electron microscope tips[4] and nanoscale electronics.[5] Anticipated applications include their use as catalyst supports,[6] hydrogen storage media,[7] and as reinforcing materials for carbon matrix composites.[8] To realize these larger scale uses will require scaleable, economical synthesis methods.

Current methods for synthesizing metal-catalyzed nanotubes (MCNTs) use either arc discharges[9−11] or high temperature furnaces.[12−16] The arc discharge provides little control over process conditions, thus producing a myriad of unwanted byproducts and a low yield.[17] In contrast, high temperature furnaces offer a high degree of control over the hydrocarbon identity, temperature, and reaction time, all of which can be optimized for product purity. However, both methods are energy intensive and produce relatively low quantities of nanotubes. Furthermore, neither method is readily scaleable for bulk commercial production.

In contrast to these methods, a flame is energy efficient, providing a source of hot hydrocarbon gas through combustion of a portion of the fuel. Particularly appealing commercial aspects of flame synthesis are the rapid time scale (on the order of tens of milliseconds[18]) on which simple gaseous precursors can be converted to solid-phase aerosols and the continuous as opposed to batch process it offers. Moreover, it is readily scaleable for commercial production as evidenced by its widespread use as an econonomical, scaleable method for the synthesis of a variety of inorganic and organic materials.[19] Perhaps the best known flame synthesis product, soot, occurs readily and is exploited in the purposeful synthesis of carbon black.[20]

A metal particle catalyst, which is integral to the arc discharge and high temperature furnace approaches, is also necessary for flame synthesis of MCNTs. A technique commonly used to create metal nanoparticle catalysts in the aerosol phase is the decomposition of an organometallic such as a metallocene. The relatively low temperatures required for thermal decomposition of ferrocene, nickelocene, or cobaltocene (<700 K)[15,16,21,22] suggest that these organometallics can be used to create a metal aerosol within a flame environment prior to the onset of soot formation, which has a temperature threshold of approximately 1300 K.[23] Furthermore, hydrocarbon pyrolysis processes do not occur significantly at these lower temperatures during the short residence times within this temperature region of the flame.

In the work reported here, we demonstrate the synthesis of metal-catalyzed single-wall nanotubes within a flame environment. In particular, we explore the relative catalytic activity of different metal nanoparticles produced by different precursors and the effects of the flame environment composition, and assess competing processes.

Experimental Section

The flame studied here was established as a gas-jet diffusion flame surrounded by the postcombustion exhaust of a rich premixed flame supported on a McKenna burner. All substances used for the diffusion flame were introduced through a 3/8-in. diameter central tube which runs through the McKenna burner bottom and terminates level with the sintered metal surface of the burner. A 3-in. long stainless steel tube with a 1-in. outer diameter served as a chimney by centering it over the central fuel tube 1 in. above the burner suface. The chimney served to stabilize the pyrolysis stream, forming a stable cylindrical "flame". Thermophoretic sampling measurements were made 1 in. above the chimney. The McKenna burner supported a fuel-rich premixed flame composed of 11.0 slm air and 1.5 slm C_2H_2 for the results presented here, although we found that equivalence ratios ranging from 1.0 to 1.62 produced qualitiatively similar results. The pyrolysis flame in the central tube was established using either C_2H_2, C_2H_4, or CO in combination with H_2, CH_4, or air along with an inert carrier (He, N_2 or Ar). The range of flow rates explored for these gases are as follows: 0-0.3 slm for C_2H_2, C_2H_4, CH_4, CO and H_2; 0-0.2 slm for air; and 0-2 slm for the inert carriers.

Introduction of the metallocene or metal acetylacetonate was achieved through sublimation. Initial experiments used rapid pyrolysis, which used the flame-generated heat to accelerate the sublimation of the metal precursor. In this case the metallocene was located within the central fuel pyrolysis tube

* Corresponding author. Phone: (216) 433-9065. Fax: (216) 433-3793. E-mail: randy@rvander.lerc.nasa.gov.

10.1021/jp994304n CCC: $19.00
Published on Web 07/19/2000

in a tungsten wire or stainless steel basket. Later experiments used temperature-controlled sublimation achieved through electric heating of a sublimation cell. In this arrangement, metallocene vapor was entrained within the inert gas that was the major component of the pyrolysis flame. Calculations based on these methods gave introduction rates that ranged from 0.1 to 5 mg/min.

Thermophoretic sampling measurements were performed using a double-action air-driven piston. The dwell time of the probe within the flame was controlled by custom electronics which actuated a dual-valve solenoid to govern the pressurized air-flow. Light scattering measurements off the probe tip were used to characterize the insertion, dwell, and retraction process. Results were well-represented by a trapezoid function with 10−15 ms insertion and retraction times with dwell times maintained so as to provide a total residence time for the probe within the flame of 200−250 ms for a single exposure. TEM grids were attached to the probe by a sandwich grid holder consisting of a 0.003-in. thick brass shim with a 2-mm diameter hole exposing both sides of the TEM grid. This grid holder was attached to the insertion rod of the probe by a small set screw.

The essential idea behind thermophoretic sampling is that material is driven to the collection surface by a temperature gradient existing between the collection surface (at low temperature) and the surrounding gas environment (at elevated temperature). Maintaining the probe residence time short so as to restrict its temperature rise is thus basic to the collection method. As the probe temperature remains much lower than that of the surrounding ambient for the duration of the exposure, the thermophoretically deposited material and possible subsequent reactions are quenched. Recent measurements by this author have shown that for the indicated sampling time durations, the probe surface temperature does not exceed 200 °C.[24] Work reported elsewhere has demonstrated this with respect to TEM analysis of "soot precursor material" similarly sampled by ourselves and others.[25,26] All samples were collected from the center axial region of the flames where radial gradients in species concentration and temperature are small.

Statements regarding the relative quantities of SWNTs are based on examination of multiple TEM images of samples from different days using the same flame conditions. The consistent results assured us that our catalyst seeding and material sampling methods were reproducible. Differences between aggregate groups of samples using either N_2 or Ar as diluent or CO as fuel were not subtle. Finally, several images from each grid confirmed the uniformity of the sampled material and the relative differences produced by the different experimental conditions.

Results

Figure 1 is a TEM micrograph at low resolution illustrating the nanotube yield within the thermophoretically sampled material. For the indicated acetylene and H_2 concentrations, several SWNTs were observed within any imaged region as represented in Figure 1. Figures 2 and 3 are intermediate and high-resolution TEM (HRTEM) micrographs illustrating the SWNT structure in more detail. Even though the acetylene concentration of greater than 10% hydrocarbon is high compared to furnace syntheses using supported catalysts, we invariably observed an absence of amorphous carbon covering the exposed sections of the nanotubes. Typical diameters of the nanotubes were between 2 and 3 nm, and observable lengths ranged between tens to hundreds of nanometers. As shown, metal nanoparticles with diameters comparable to those of the single-walled nanotubes were also present and appeared to be entombed within a carbonaceous matrix. Only rarely was a metal catalyst particle observed at the tip of a nanotube, as shown in Figure 4. Encapsulation of the catalyst particle is consistent with the termination of the SWNT growth. The nanotubes themselves were sensitive to the electron beam beyond a minute of exposure. Additional exposure resulted in crumpling deformations which rapidly led to breakage.

Tests for the effect of the flame environment upon nanotube synthesis were performed and yielded several insights. First, the presence of fuel within the pyrolysis flame was essential to the formation of nanotubes when using cobaltocene or ferrocene. Only very rarely was a nanotube observed when using any metal precursor without fuel. On the basis of the relative nanotube yield as observed through TEM images, acetylene was 10-times more reactive than ethylene towards nanotube formation in the presence of hydrogen. Changing the identity of the hydrocarbon fuel to CO resulted in nanotubes with lengths in excess of a micron. Substitution of Ar for nitrogen as the inert carrier within the pyrolysis flame decreased the relative nanotube yield for a given acetylene and hydrogen concentration. Finally, within the pyrolysis flame, the relative nanotube yields were found to be independent of the fuel/air equivalence ratio of the surrounding rich premixed flame. Fuel−air equivalence ratios between 1.0 and 1.6 did not alter the average number of observed nanotubes when using the indicated pyrolysis flame conditions.

Changes in the individual concentrations of acetylene or H_2 in general decreased the relative yield of SWNTs. Increased concentrations of either C_2H_2, C_2H_4 or CO appeared to increase the yield of carbonaceous matrix around the catalyst particles, especially in the case of C_2H_2. It also dramatically reduced the yield of SWNT, especially when using cobalt acetoacetonate. Decreased concentrations of these gases also appeared to lead to fewer SWNTs, although the effect was less dramatic than that observed with increased fuel concentration. The SWNT yield appeared rather independent of the CO concentration but the lengths appeared to increase with increasing concentration. Hydrogen was found to be a critical synergistic agent for appreciable nanotube growth with acetylene, though not with ethylene. Small changes in the H_2 concentration had no observable effect, but large increases led to a decreased SWNT yield. Simultaneous increases or decreases in acetylene and H_2 concentration had a lesser effect upon SWNT yield than did varying the two concentrations independently. SWNTs were still observed when using air or CH_4 in place of fuel in the central flame, though in far less abundance than when acetylene and H_2 were used. Finally, although difficult to quantify, relative reactivity toward SWNT formation was greatest for cobalt acetoacetonate, with cobaltocene and ferrocene exhibiting a lesser activity that was comparable for each of the two compounds. Copper acetylacetonate did not result in MCNT formation. It should be noted that the observed relative reactivities may reflect more upon the flame conditions than upon the inherent reactivity of the catalyst metal nanoparticles.

Figure 5 shows the structure of the carbonaceous material in which many metal particles were embedded. Although nearly all of the metal particles are within a size range suitable for catalyzing small MWNTs consisting of a few carbon layers, they apparently did not do so. The particle size distribution within the matrix was rather uniform. The average particle size was found to be approximately 5 nm, the average of 30 particles. Moreover, the particles appeared individually separated, exhibiting no aggregation.

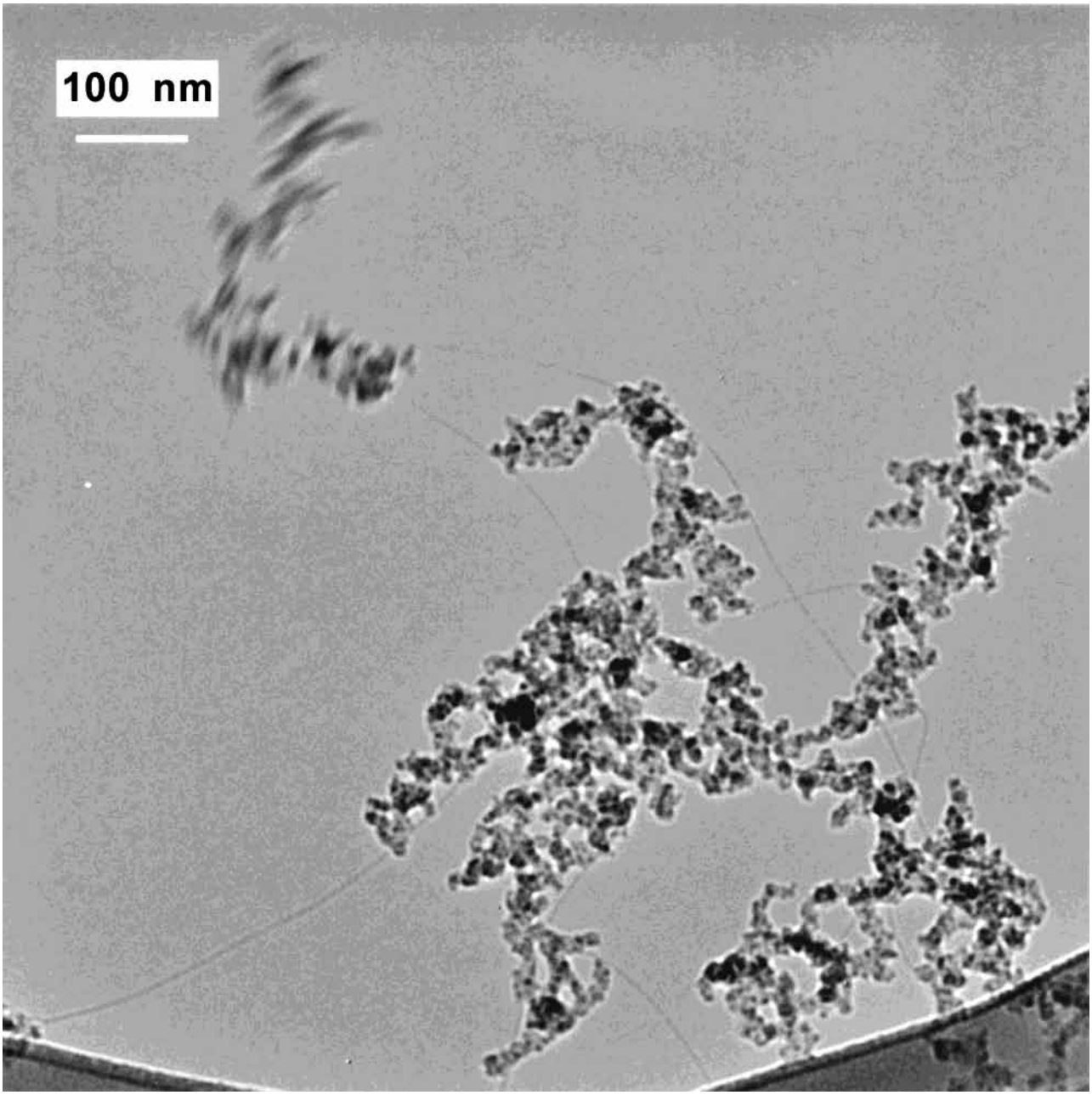

Figure 1. A low-magnification TEM micrograph illustrating the relative abundance of metal-catalyzed carbon nanotubes and carbonaceous matrix.

Discussion

Flame Environment. The independence of the nanotube yield upon the fuel/air ratio of the surrounding premixed flame is consistent with the observation that the postcombustion gases of this flame form the outer hot gas mantle surrounding the central flame. Stable combustion products, assorted aromatic compounds, and soot all comprise this surrounding gas stream. None of these species is known to be active in catalytic nanotube formation, a result supported by the independence of the nanotube synthesis upon the surrounding premixed flame equivalence ratio. Given that measured temperatures within this product stream were less than 1000 K, reactive radical species (such as OH) concentrations are considered inconsequential given their minuscule concentration at these temperatures.

The dependence of nanotube formation on the simultaneous presence of acetylene and hydrogen indicates that these are the dominant growth species for nanotube formation. Acetylene has a far greater propensity for dissociative adsorption than ethylene upon transition metals due to the reaction exothermicity. Additionally, the evolved heat may accelerate the carbon solution within the metal nanoparticle. For the concentrations, residence times, and temperature used here, only a portion of the ethylene is expected to pyrolyze to acetylene, in addition to other pyrolysis products. The lower acetylene concentration would then account for the observed lower SWNT yield with ethylene if the in-situ generated acetylene were the active agent in the SWNT formation. The absence of SWNTs in the absence of fuel indicates that the cyclopentadienyl moiety of the metallocence or its decomposition products were not the (main) carbon source for the nanotubes. However, we note that these species could act synergistically with acetylene and hydrogen to promote the nanotube growth.

The necessary presence of H_2 can be attributed to a combination of its ability (a) to selectively etch amorphous carbon, (b) to aid in surface restructuring, and (c) to interact with adsorbates. The ability of atomic hydrogen to selectively etch amorphous

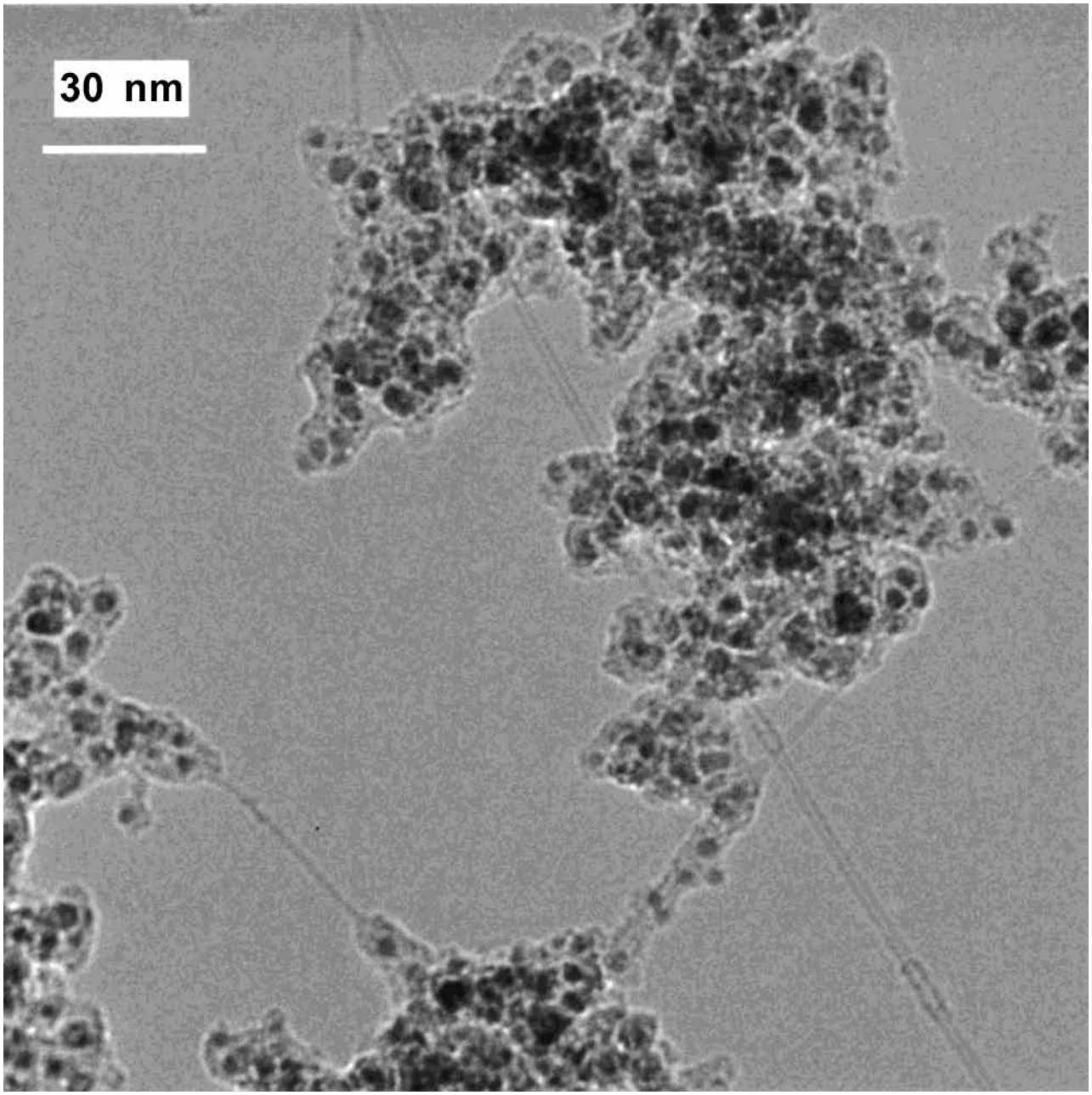

Figure 2. An intermediate-magnification TEM micrograph illustrating the SWNT structure and typical particle sizes within the carbon matrix.

carbon is well-known from diamond film growth studies.[27] Molecular hydrogen could perform a similar function removing amorphous carbon from the catalyst particle surface thereby maintaining the accessiblity of active catalytic sites. Through electronic structure effects (changing the local electron density) molecular hydrogen can facilitate metal surface restructuring at elevated temperatures.[28] Molecular hydrogen has also been observed to either promote or inhibit the adsorption of CO on transition metals, depending upon its concentration.[29] The relative contributions of these factors is not resolvable in these experiments. Notably, methane and oxygen can increase the hydrocarbon radical concentration within fuel-rich, pyrolysis regions.[30,31] These radicals may contribute to SWNT growth directly through enhanced decomposition rates upon adsorption or indirectly by increasing the hydrogen and acetylene concentrations.

The dependence of the nanotube growth on inert gas reflects a sensitivity to reactant concentration, thermal conductivity, and possibly collision partner in intermediate reaction steps. Since Ar and N_2 have similar thermal conductivities and diffusivities, the lower SWNT yield obtained with Ar at similar concentrations with N_2 may reflect the effect of collision partner in a three-body reaction. Alternatively, with the identical concentrations used to establish the two flames, the differences more likely reflect the thermal capacities of the inerts. For the indicated concentrations, the average flame temperature on the centerline is more than 100 °C higher with Ar as diluent than with N_2 based on calculated flame temperatures for the given level of inert added. That the nanotube yield decreases with elevated temperature is not consistent with temperature driven kinetics. Indeed, the rates of hydrocarbon dissociative adsorption, carbon solution, and diffusion of carbon through the catalyst particle will all increase with increasing temperature. However, the rate of formation of large polyaromatic hydrocarbons (PAHs) and consequently their concentration will also increase with increasing temperature. Given their thermodynamic stability[32] and resistance to catalytic decomposition, PAHs are not expected to readily undergo dissociative adsorption. Hence the decline

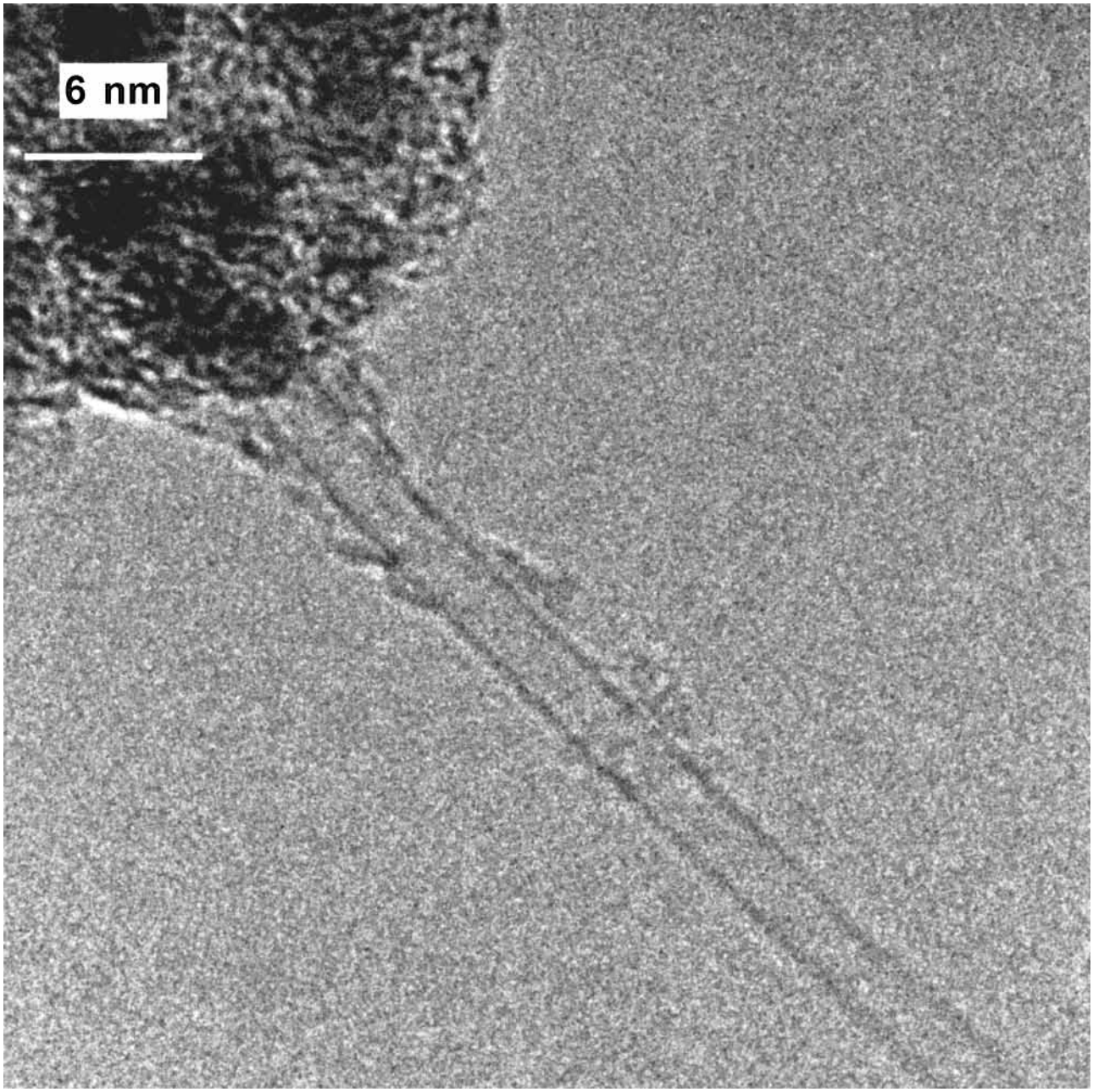

Figure 3. A high-magnification TEM micrograph showing the absence of pyrolytic material upon the SWNT wall.

in nanotube yield is interpreted as reflecting the increased rate of deactivation of the catalyst particles at the elevated temperatures by PAHs.

Higher inert gas concentrations (and correspondingly lower acetylene and hydrogen concentrations) led to a lower yield of nanotubes. This suggests that the nominal concentrations used (as described in the experimental section) are within a reactant-limited synthesis regime. This effect is especially dramatic for CO, for which higher concentrations led to longer SWNTs with little change in yield.

Higher hydrocarbon concentrations, obtained by adding more acetylene to the pyrolysis flame, produced fewer nanotubes. Correspondingly, the carbonaceous matrix which contained many metal nanoparticles became increasingly amorphous. Similar results were obtained by increasing the hydrogen concentration. While higher hydrocarbon concentrations may lead to accelerated nanotube growth, the loss of metal nanoparticles through encapsulation or encasement of developing nanotubes appears to effectively compete, resulting in a lower nanotube yield under these conditions. Indeed, at higher acetylene concentrations, an amorphous carbon layer was observed on the single-wall nanotubes as illustrated in Figure 1, (low- resolution TEM image). Higher H_2 concentrations likely decrease SWNT yields by a simple dilution effect. Higher H_2 concentrations could also more effectively terminate dangling carbon bonds and radicals, possibly increasing the yield of amorphous carbon relative to graphitic carbon.

Encapsulation. As can be seen from the overview images shown in Figures 1 and 2, a large percentage of metal nanoparticles do not catalyze the formation of a nanotube but rather are encased within a carbonaceous matrix. Figure 5 is a HRTEM micrograph illustrating the partial graphitization surrounding the entombed metal nanoparticles. The formation of nanotubes from particles of similar size as those that are embedded suggests that the nanotubes were formed at least concurrently if not prior to encapsulation of the majority of metal nanoparticles. Hence the "burial" of these particles raises the question as to whether they were entombed before or during

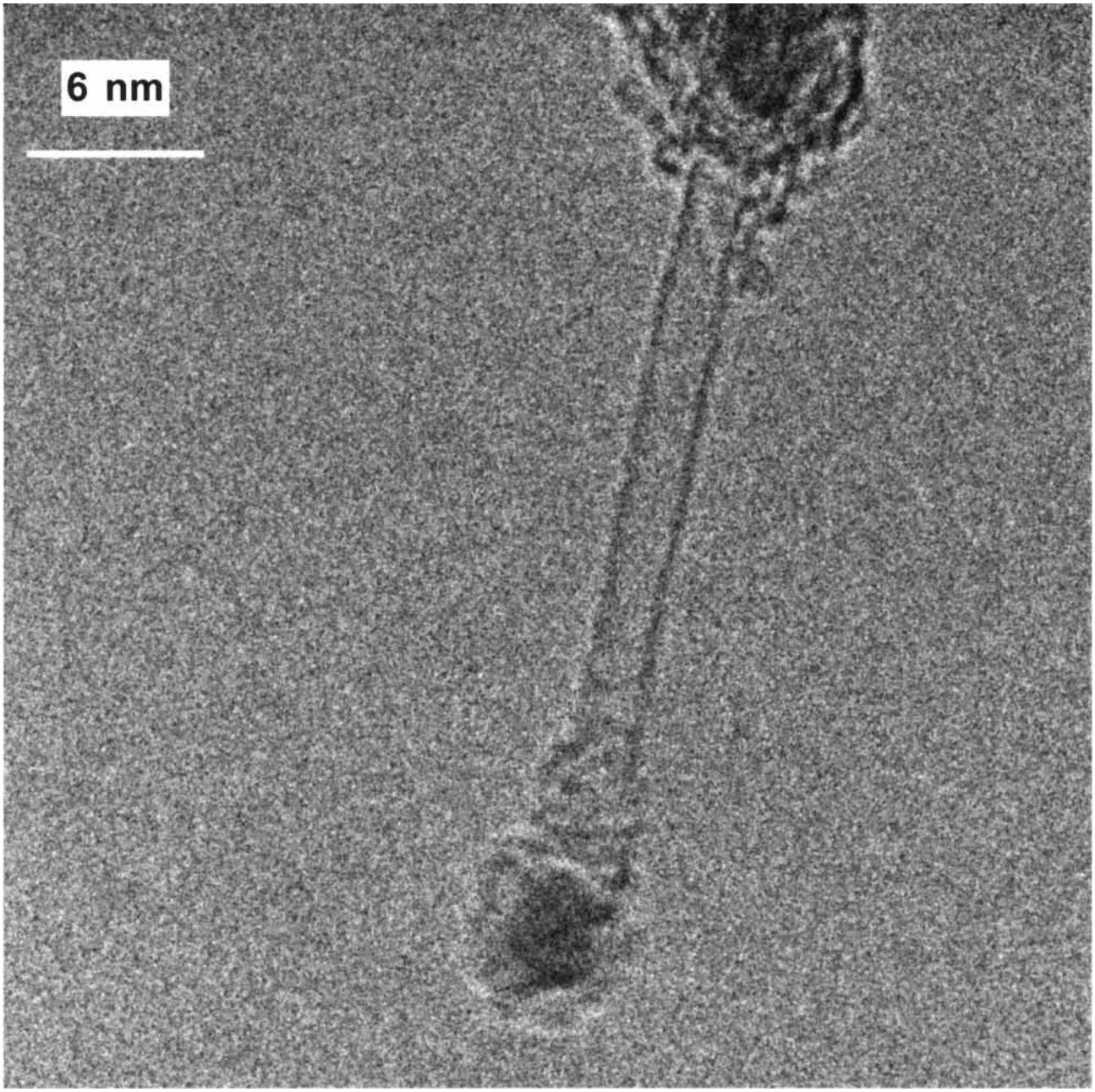

Figure 4. A high-magnification TEM micrograph of a SWNT and catalyst particle prevented from further growth by encapsulation of the catalyst particle.

initial stages of catalyzed nanotube growth or whether they were inactive toward nanotube formation from their inception and eventually became encased.

It is possible that many particles are inactive toward nanotube formation given their formation history. The decomposition of the metallocene and clustering of the metal atoms occurs at temperatures well below the bulk metal sintering or melting temperatures. Hence the clusters may not be created in an energetically stable, crystallographic form. Consequently, the nascent metal nanoparticle may possess numerous surface steps and lattice defects.

Both physical geometry and the altered electronic structure (electron density) arising from this defect structure may render the particle less facile at decomposing adsorbed hydrocarbons or precipitating dissolved carbon as graphitic layers. For example, lattice steps and dislocations would likely pose steric inhibitions toward a species which adsorbs by bridging surface lattice planes and may restrict access to reactive sites for species for which end-on adsorption is energetically preferable. The local electron density which interacts with that of the adsorbate would undoubtedly be perturbed by such irregularities in the surface structure.

The effect of irregular surface structure or unsuitable electronic structure would be most pronounced for the smallest metal nanoparticles capable of only forming a single-wall nanotube. A single lattice defect or irregular surface step could dramatically interfere with the carbon precipitation and potentially prevent orderly carbon dissolution required for nanotube growth particularly at the rear facets of the particle, where the single-wall nanotube can only arise through carbon precipitation from specific physical locations, interstitially located between lattice planes.

The dissociative decomposition of PAHs and other relatively stable adsorbing species is likely to be particularly sensitive to geometric or electronic alterations in the metal particle or to decreased ease of carbon dissolution. Thus, encapsulation of

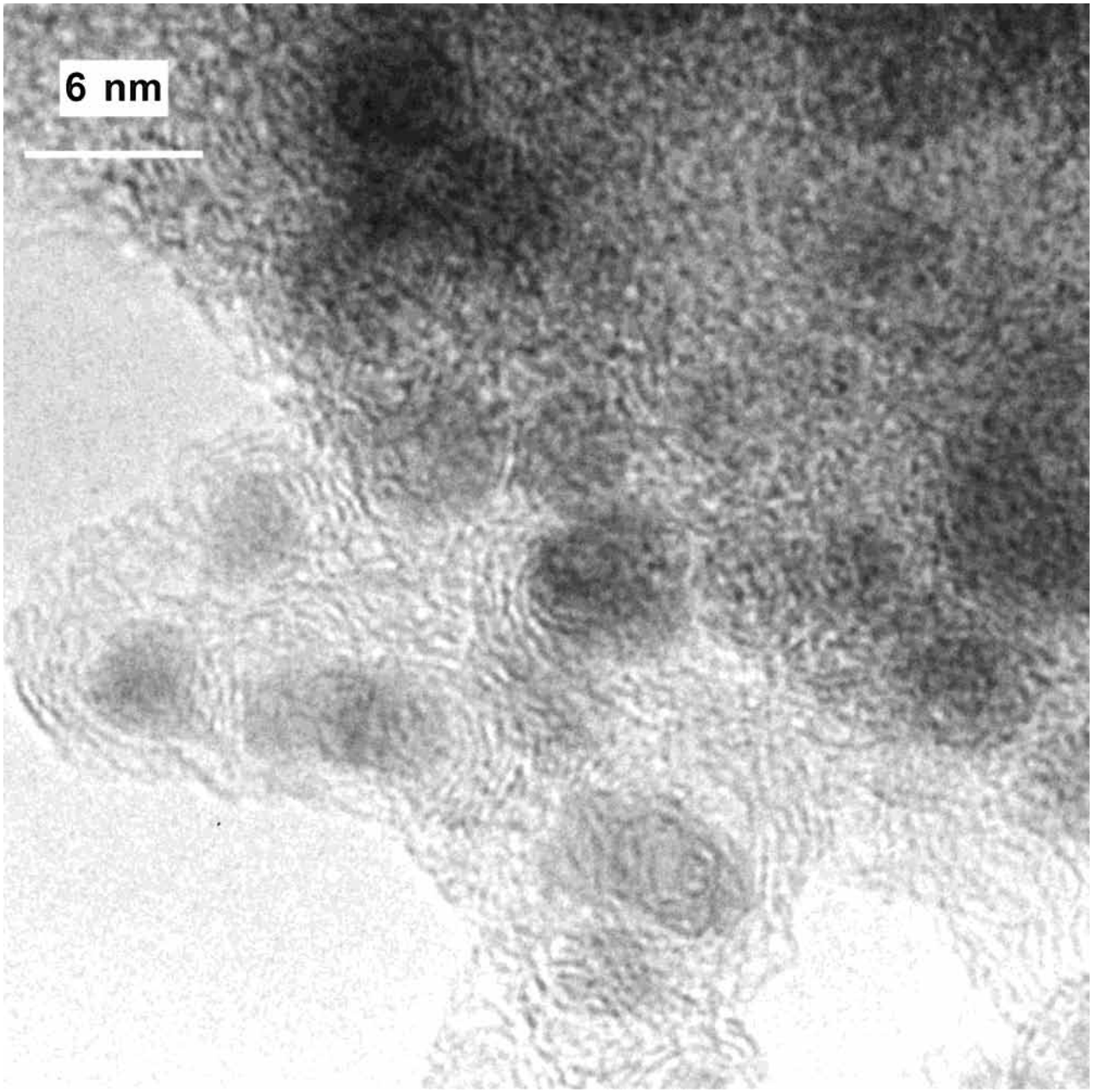

Figure 5. A high-magnification TEM micrograph of entombed cobalt metal catalyst particles and carbonaceous matrix.

the metal nanoparticle rather than nanotube growth would be accelerated. Although some restructuring may occur within the reducing flame environment, it is unclear if the residence time, temperature, and hydrocarbon environment would be sufficient to bring about the necessary restructuring prior to encapsulation. Consistent with this mechanism is the observed absence of SWNTs produced by laser ablation methods within high temperature furnaces at temperatures lower than 1000 °C.[33]

A second possibility for the encapsulation of the majority of metal particles is that most of the metal particles never had a chance to begin nanotube formation despite the availability of a surface with suitable crystallinity, electronic structure, and corresponding reactivity. In this case, the entrapment within the carbonaceous matrix could reflect a high hydrocarbon concentration such that the rate of deposition on the metal particle would exceed the rate of carbon solvation or dissolution. Effectively the particle becomes a seed for soot inception and growth.

Such a process would be highly dependent upon the local hydrocarbon environment. Large polyaromatic hydrocarbons (PAHs), species that are known to be thermodynamically stable and relatively inactive toward catalytic decomposition, may deactivate the particle by blocking surface sites before nanotube growth could begin. If the concentration were sufficiently high, deposition of PAHs would be expected on all nanostructures within the flame. However, the lack of pyrocarbon deposition upon the nanotube surfaces is inconsistent with this mechanism of encapsulation (catalyst deactivation) and suggests that the encapsulation is not dominated by a large gas-phase concentration of PAHs. Recall that our experimental results suggest that the optimal pyrolysis flame concentrations observed are within a reactant-limited supply regime. In addition, the carbon matrix in which the particles reside is not truly amorphous, as would be expected if this mechanism were operative as discussed below.

A third possibility is that the encapsulation results from the metal nanoparticle being too catalytically active toward adsorptive decomposition of hydrocarbons. Close inspection of the surrounding carbon matrix, illustrated in Figure 5, reveals that much of the carbon host matrix is locally graphitic. The metal nanoparticles appear to be nested within 2−4 partially graphitized carbon lamella as illustrated by the extended carbon layer planes in the lattice fringe image of Figure 5. Beyond these segments, the surrounding carbon was amorphous. In this case, the particles are too active toward hydrocarbon decomposition. In this scenario, irregularities in the surface lattice plane structure and local electron density may actually promote this "reactive encapsulation". Note that this deactivation mechanism is opposite to the first mechanism for encapsulation we proposed.

Support for this mechanism arises from studies of metal−soot interactions within flames. The surface-catalyzed dehyrogenation of acetylene leading to PAHs remaining attached to iron nanoparticle surfaces was postulated by Retreivi et al. to account for the soot-promoting effect of ferrocene within premixed flames.[34] Layered, in-situ formation/deposition of large aromatic compounds is consistent with the observation of extended graphitic lamella seen in the high-resolution image. The formation of ordered turbostratically stacked carbon layer planes would then also provide a template for subsequent growth at reactive edge sites through the well-known hydrogen abstraction, acetylene addition mechanism that describes PAH and soot growth within flames.[35,36] In this manner the turbostratic layer-plane structure could be retained, at least initially. With increasing residence time within the flame environment, the large variety of hydrocarbon fuel pyrolysis products (including PAHs) obtained and the high surface collision rates could well disrupt the orderly growth of graphitic layer-plane segments, leading at best to extended graphitic lamella, as observed here and in ordinary soot.

We note that an amorphous metal particle may be too active toward hydrocarbon decomposition relative to carbon solvation. The surface metal atoms may be deficient in electron density relative to those within the bulk. Thus their d-shell orbitals may easily establish orbital overlap with the electron-rich hybrid orbitals of unsaturated hydrocarbons while their lack of crystalline structure impedes the following steps of carbon solvation and diffusion through the particle and subsequent precipitation.

A significant source of encapsulating material may be the cyclopentadienyl radicals arising from the metallocene decomposition. While the cyclopentadienyl radical itself is resonantly stabilized, it is likely to be highly reactive toward hydrogenation or bond formation. Through hydrogenation, the ring achieves thermodynamic stability and will become resistant to catalytic decomposition. Through bonding such as may be achieved by orbital overlap with the valence electron band of a metal particle, the radical may avoid decomposition in the gas phase. Five-membered rings have been found experimentally and theoretically to accelerate PAH growth by advancing naphthalene formation, a critical step in the formation of larger PAHs.[37] If this were a dominant process, then acetylacetonate would be expected to result in far fewer encapsulated catalyst particles. While qualitative visual observations do not reveal dramatic differences in the number of entombed catalyst particles and consequently do not support this hypothesis, the observation of a greater yield of SWNTs with cobalt acetylacetonate does indirectly support the deactivation of the catalyst particles through the cyclopentadienyl radical.

In summary, the rapid encasement of most of the metal nanoparticles can be attributed to the catalytic inactivity of at least some of the nanoparticles, the deposition of cyclopentdienyl radicals, molecules, and other thermodynamically stable species, and by the unfavorably high catalytic activity of some of the particles toward surface PAH formation. The avoidance of flame temperatures and fuel identities and concentrations leading to significant PAH formation are then parameters to be optimized in order to realize higher flame synthesis yields.

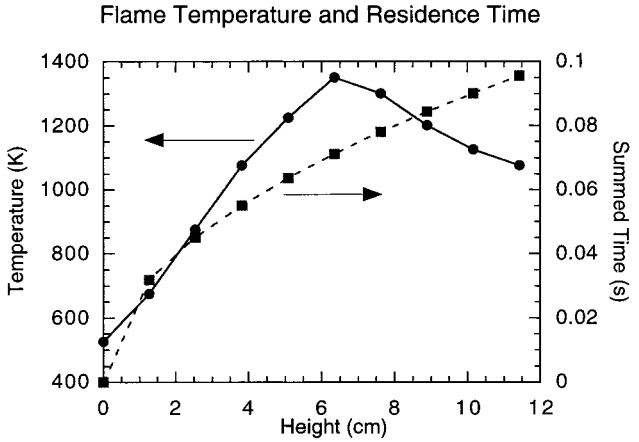

Figure 6. A plot of measured temperature (circles) along the axial streamline within the pyrolysis flame and calculated integrated residence time (squares) within the flame (along this streamline) as a function of height within the flame.

Figure 6 plots the measured flame temperature profile along the axial streamline of the diffusion flame and a cumulative residence time within the flame along this streamline on the basis of buoyantly accelerated convection.[38] As seen from the figure, the total time for nanotube formation within the flame is less than 100 ms. This calculated time does not differentiate between the time required for metallocene decomposition, metal nanoparticle formation, and nanotube growth. Hence, it is a conservative estimate of the time required for SWNT growth. With this time and measured nanotube lengths of hundreds of nanometers, a minimum average growth rate of 1000 nm/s is calculated. This rate is an order of magnitude faster than that based on process tube diameters and flow rates[12−15] within high temperature furnaces and illustrates the high potential of flame synthesis for large scale commercial production of nanotubes.

Argument for Gas-Phase Nanotube Growth. An alternative explanation for the nanotubes formed is that they arise from carbon dissolution, diffusion, and precipitation from the amorphous carbon in which the particle is embedded. These particles are catalytically active as evidenced by the partial graphitization of the surrounding carbon. If true, then a far larger number of nanotubes would be expected given the vast number of embedded particles relative to the nanotubes, even if only embedded particles near the edges of the amorphous carbon were able to create a nanotube from surrounding material. Second, the interaction between the embedded particles and the surrounding amorphous carbon observed is that of graphitization. The material surrounding the particles, as shown in Figure 5, is partially graphitized compared to that material not in the vicinity of any nanoparticle. The graphitic lamella are circumferential, consistent with the proposed encapsulation mechanism. No evidence of particle tunnels or graphitic segments oriented toward the boundary of the carbonaceous matrix is observed. Additionally, no filaments, short nanotube stubs, or growths of any kind are observed along the border of the carbon−metal nanoparticle composite. TEM imaging of material samples collected upstream (earlier in growth history) also do not reveal any such hints of such nanotube formation that conceivably

might have been covered at later times within the flame. Rather, the extended graphitic lamella are always observed, even at the earliest stages, supporting the proposed encapsulation mechanisms discussed above.

Conclusions

Flame synthesis of metal-catalyzed carbon nanotubes has been demonstrated. Their synthesis is critically dependent upon both the fuel identity and concentration and on the presence of hydrogen. Concentrations of 10% acetylene and 10% hydrogen within a nitrogen carrier yielded the most single-wall MCNTs based on a preliminary survey. Carbon monoxide proved uniquely synergistic toward the formation of very long single-walled MCNTs. The use of additives within the fuel other than H_2, such as CH_4 and air, still resulted in nanotube synthesis, albeit in much lower yields. A wide range of catalyst metal particles are effective toward MCNT formation within this environment. As precursors to the catalyst metal nanoparticles, the order of reactivity based on relative nanotube yield is cobalt acetylacetonate > cobaltocene ~ ferrocene. As expected from literature reports, copper did not catalyze nanotube formation.

Initial results also reveal that a large fraction of the catalyst particles are entombed within a carbonaceous matrix. Possible mechanisms for this internment include blockage of active surface sites by thermodynamically stable species, ill-formed catalyst particles which are unreactive in their amorphous state, or highly active particles that accelerate the formation of an encapsulating graphitic layer relative to the rate of carbon solution or precipitation. Finally, because flame synthesis has a demonstrable history of scalability for high volume synthesis, the method holds promise in this regard.

Acknowledgment. This work was administered through NASA cooperative agreement NAC3-544 with The National Center for Microgravity Research on Fluids and Combustion for a NASA NRA combustion award (RVW). Prof. Ticich and Ms. Curtis acknowledge support through the Ohio Aerospace Institute Collaborative Aerospace program for visiting summer faculty and accompany students. The authors gratefully acknowledge David R. Hull (GRC) for the TEM imaging.

References and Notes

(1) Mintmire, J. W.; Dunlap, B. I.; White, C. T. *Phys. Rev. Lett*. **1992**, *68*, 631.

(2) Saito, R.; Fujita, M.; Dresselhaus, G.; Dresselhaus, M. M. *Appl. Phys. Lett*. **1992**, *60*, 2204.

(3) Walters, D. A.; Ericson, L. M.; Casavant, M. J.; Liu, J.; Colbert, D. T.; Smith, K. A.; Smalley, R. E. *Appl. Phys. Lett*. **1999**, *74*, 3803.

(4) Wong, S. S.; Harper, J. D.; Lansbury, P. T., Jr.; Lieber, C. M. *J. Am. Chem. Soc*. **1998**, *120*, 603.

(5) Collins, P. G.; Zettl, A.; Bando, H.; Thess, A.; Smalley, R. E. *Science* **1997**, *278*, 100.

(6) Planeix, J. M., et al. *J. Am. Chem. Soc.* **1994**, *116*, 7935.

(7) Dillon, A. C. *Nature* **1997**, *386*, 377.

(8) Treacy, M. M. J.; Ebbesen, T. W.; Gibson, J. M. *Nature* **1996**, *381*, 678.

(9) Kiang, C.-H.; Goddard, W. A., III; Beyers, R.; Salem, J. R.; Bethune, D. S. *J. Phys. Chem*. **1994**, *98*, 6612.

(10) Lin, X.; Wang, X. K.; Dravid, V. P.; Chang, R. P. H.; Ketterson, J. B. *Appl. Phys. Lett*. **1994**, *64*, 181.

(11) Cassell, A. M.; Scrivens, W. A.; Tour, J. M. *Chem. Mater*. **1996**, *8*, 1545.

(12) Mukai, S. R.; Masuda, T.; Fujikata, Y.; Hashimoto, K. *Carbon* **1996**, *34*, 645.

(13) Guo, T.; Nikolaev, P.; Thess, A.; Colbert, D. T.; Smalley, R. E. *Chem. Phys. Lett*. **1995**, *243*, 49.

(14) Satishkumar, B. C.; Govindaraj, A.; Rao, C. N. R. *Chem. Phys. Lett*. **1999**, *307*, 158.

(15) Cheng, H. M.; Li, F.; Su, G.; Pan, H. Y.; He, L. L.; Sun, X.; Dresselhaus, M. S. *Appl. Phys. Lett*. **1998**, *72*, 3282.

(16) Andrews, R.; Jacques, D.; Rao, A. M.; Derbyshire, F.; Qian, D.; Fan, X.; Dickey, E. C.; Chen, J. *Chem. Phys. Lett*. **1999**, *303*, 467.

(17) Dravid, V. P.; Host, J. J.; Teng, M. H.; Elliot, B.; Hwang, J.; Johnson, D. L.; Mason, T. O.; Weertman, J. R. *Nature* **1995**, *374*, 602.

(18) Santoro, R. J.; Yeh, T. T.; Horvath, J. J.; Semerjian, H. G. *Combust. Sci. Technol*. **1987**, *53*, 89.

(19) Howard, J. B. Fullerenes formation in flames. *The Twenty-Fourth Symposium (International) on Combustion*; The Combustion Institute: Pittsburgh, PA, 1992; p 933.

(20) *Carbon Black Science and Technology*, 2nd ed.; Donnet, J. B., Bansal, R. C., Wang M.-J., Eds.; Marcel Dekker: New York, 1993.

(21) Ishioka, M.; Okada, T.; Matsurbara, K.; Endo, M. *Carbon* **1992**, *30*, 865.

(22) Sen, R.; Govidndaraj, A.; Rao, C. N. R. *Chem. Phys. Lett*. **1997**, *267*, 276.

(23) Glassman, I. *The Twenty-Seventh Symposium (International) on Combustion*; The Combustion Institute: Pittsburgh, PA, 1998; p 1589.

(24) Vander Wal, R. L.; Householder, P. A.; Wright, T. W., III. *Appl. Spectrosc*. **1999**, *53*, 1251.

(25) Vander Wal, R. L. *Combust. Flame* **1998**, *112*, 607.

(26) Dobbins, R. A. *Combust. Flame* **1995**, *100*, 301.

(27) Wang, X. K.; Lin, X. W.; Mesleh, M.; Jarrold, M. F.; Dravid, V. P.; Ketterson, J. B.; Chang, R. P. H. *J. Mater. Res*. **1995**, *10*, 1977.

(28) Rodriguez, N. M.; Kim, M. S.; Baker, R. T. K. *J. Catal*. **1993**, *144*, 93.

(29) Herreyre, S.; Gadelle, P. *Carbon* **1995**, *33*, 234.

(30) Senkan, S.; Castaldi, M. *Combust. Flame* **1996**, *107*, 141.

(31) Hwang, J. Y.; Chung, S. H.; Lee, W. *The Twenty-Seventh Symposium (International) on Combustion*; The Combustion Institute: Pittsburgh, PA, 1998; p 1531.

(32) Stein, S.; Fahr, A. *J. Phys. Chem*. **1985**, *89*, 3714.

(33) Yudasaka, M.; Yamada, R.; Sensui, N.; Wilkins, T.; Ichihashi, T.; Iijima, S. *J. Phys. Chem*. **1999**, *103*, 6224.

(34) Ritrievi, K. E.; Longwell, J. P.; Sarofim, A. F. *Combust. Flame* **1987**, *70*, 17.

(35) Wang, H.; Frenklach, M. *Combust. Flame* **1997**, *110*, 173.

(36) Frenklach, M.; Wang, H. *The Twenty-Third Symposium (International) on Combustion*; The Combustion Institute: Pittsburgh, PA, 1990; p 1559.

(37) Marinov, N. M.; Castaldi, M. J.; Melius, C. F.; Tsang, W. *Combust. Sci. Technol*. **1997**, *128*, 295.

(38) McEnally C. S.; Pfefferle, L. D. *The Twenty-Seventh Symposium (International) on Combustion*; The Combustion Institute: Pittsburgh, PA, 1998; p 1539.